Electronic Supplementary Material (ESI) for ChemComm.

Supplementary Information

A structurally precise Ag_xAu_{25-x} nanoclusters based cancer theranostic platform with tri-targeting/in-situ O_2-generation/aggregation enhanced fluorescence imaging/photothermal-photodynamic therapies

Ying Yang, Yinlong Zhou, Shuxin Wang, Xueyan Wang, Xuan Liu, Anjian Xie, Yuhua Shen, and Manzhou Zhu**

College of Chemistry and Chemical Engineering, Institute of Physical Science and Information Technology, Anhui University, Hefei 230601 (P.R. China)

E-mail: s_yuhua@163.com, zmz@ahu.edu.cn

Experimental section

Main materials

Hyaluronic acid (HA, 400 kDa), anhydrous ferric chloride ($FeCl_3$), octadecylamine (OA), folic acid (FA), 1, 3-diphenylisobenzofuran (DPBF), 1-ethyl-3-(3-dimethylaminopropyl) carbodiimide (EDC), N-hydroxysuccinimide (NHS) and pyrene were got from Aladdin Reagent Co., Ltd. Tetrachloroauric(III) acid ($HAuCl_4 \cdot 3H_2O$), silver nitrate ($AgNO_3$), triphenylphosphine (PPh_3), phenethyl mercaptan (PET) and sodium borohydride ($NaBH_4$) were received from Macklin Reagent Co., Ltd. Hydrogen peroxide (H_2O_2), methanol (MeOH), anhydrous ethanol (EtOH), dichloromethane (DCM), dimethyl sulfoxide (DMSO), and N, N-dimethylformamide (DMF) were bought from Sinopharm Chemical Reagent Co., Ltd. Biomedical agents were got from Sigma-Aldrich Reagent Co., Ltd., USA. Deionized water (DI water, Milli-Q, resistivity: 18.2 MΩ•cm) was used throughout the work. All reagents were used without further purification.

Characterization

Transmission electron microscopy (TEM) images of samples were gained with a JEM-2100 (Japan Electronics, Japan) transmission electron microscope under an acceleration voltage of 200kV. Fourier transform infrared (FT-IR) spectra were obtained on a NEXUS-870 spectrometer (Thermo Fisher Scientific, USA). Ultraviolet visible (UV-Vis) absorption spectra of samples were performed by a UV-3900 UV spectrophotometer (Hitachi, Japan). Fluorescence spectra were performed with a SOL confocal fluorescence microscope (Confotect MR520, Belarus). The zeta potentials and diameters of the products were determined on an ELSZ-2 (Otsuka Electronics, Japan) zeta potential and particle size analyzer. A CW diode laser (LSR808NL-2000) with a wavelength of 808 nm was used for the laser irradiation experiments. An intelligent portable instrument (Heng Xin AZ8403) was employed for measuring the amount of dissolved O_2 in the phosphate buffer solution (PBS).The OD values of 3-(4, 5-dimethyl-2-thiazolyl)-2, 5-diphenyl-*2H*-tetrazolium bromide (MTT) assay were measured by a RT-2100C spectro-photometric micro-plate reader (Rayto, P. R. China). Fluorescence images were recorded on a DMI3000B inverted

fluorescence microscope (Leica, German). Confocal laser scanning microscope (CLSM) images were captured using an Olympus FluoView™ FV1000 confocal microscope with 60×oil immersion objective. The in vivo FL imaging photos was caught using a small animal in vivo optical imaging system (IVIS LuminaLT).

Synthesis of FHO-Fe^{3+}

100mg of EDC and 60mg of NHS were successively added into homogeneous DMF solution of HA (20 mg/mL) at room temperature. For a 2h stirring, 200mg of OA dissolved in DMF was added for conjugation with activated HA and stirred for 5h under a N_2 environment at 60 °C, then stirred at 25℃ for an extra 24 h. After the reaction, the acquired sample was dialyzed using a dialysis membrane (MWCO: 3.0 kDa) for 72 h with 5 times exchange of 4L solution of fresh DI water (30%) and EtOH (70%) to dislodge co-products. Finally, the product HO was received after freeze-dried. 100mg FA dissolved in 5mL DMSO was activated by a two-molar excess of EDC and NHS for 5h, followed by adding 50mg of HO in DMF and stirred under a N_2 environment for 6 h, the FA-HO (FHO) was finally obtained after dialyzed and freeze-dried. The FHO was further mixed with an appropriate amount of $FeCl_3$ under the condition of weak acid, so that the Fe^{3+} are coordinated with the carboxyl group on the polymer derivative, followed by dialyzed and freeze-dried to get the end product (FHO-Fe^{3+}). The critical micelle concentrations (CMC) of the HO, FHO and FHO-Fe^{3+} in DI water were tested by fluorescence measurement using pyrene as a probe.[1]

Determination of the graft ratio (GR, %) of FA on HO

The standard curve of FA was prepared at first. 5mg of FA was dissolved in 10mL of DMSO to obtain a FA stock solution (0.5 mg/mL). Take an appropriate amount of FA stock solution and dilute them with acetic acid-sodium acetate buffer (pH 5.6) to a standard solution with mass concentrations of 0.5, 1, 2, 5, 10, 20, 50 μg/mL, respectively. The absorbance is measured at 360 nm with an UV-Vis spectrophotometer and a standard curve with FA concentration versus absorbance at 360nm was obtained. Then, the appropriate amount of FHO polymer was dissolved in 10 mL of DMSO and its absorbance at 360 nm was measured. The concentration of FA was calculated using the corresponding standard curve (Fig. S1).

The GR can be measured by calculating the number of FA grafted per 100 glucose units.[2]

Synthesis of Ag_xAu_{25-x} nanoclusters (NCs)

The oil-soluble Ag_xAu_{25-x} NCs were fabricated based on our previous work.[3] Firstly, we need to synthesis the $[Au_{11}(PPh_3)_8Cl_2]^+$ and phenethylthiosilver (PhC_2H_4SAg), as two precursors for the preparation of Ag_xAu_{25-x} NCs. In brief, 0.4 mL of $HAuCl_4 \cdot 3H_2O$ aqueous solution (0.2 g/mL) was add to 10 mL of EtOH, followed by the addition of PPh_3 (0.16g), the solution is immediately clear and turned to a white suspension after about one minute. Then, 0.019 g of $NaBH_4$ dissolved in 2mL of EtOH was added. The solution quickly changed from white to bright red, and the reaction lasted for about 2 hours. The crude product $[Au_{11}(PPh_3)_8Cl_2]^+$ was obtained and purified with multiple washing of mixed DCM/hexane solvents. As for the preparation of PhC_2H_4SAg, 1 mL of $AgNO_3$ aqueous solution (0.21 mM) was added to 5 mL of EtOH with medium stirring. Then, a mixed solution of 0.6 mL of PET, 2 mL of triethylamine and 5mL of EtOH was dropped slowly into the above metal salt solution under rapid stirring. After continuing to stir for 30 minutes, the resulting precipitate was centrifuged and washed by ethanol/water multiple times to remove excess PET and other reaction by-products. The resulting product (PhC_2H_4SAg) is dried under vacuum and kept away from light. Finally, $[Au_{11}(PPh_3)_8Cl_2]^+$ was reacted with PhC_2H_4SAg to obtain Ag_xAu_{25-x} NCs. PhC_2H_4SAg (80 mg) was added to an Au_{11} NCs (75 mg)/10 mL EtOH solution under vigorous stirring at 40℃. After 6 h, the product was dried under vacuum, washed several times with EtOH/hexane (1:3, V/V), redissolved in a minimal amount of MeOH, and passed through a Sephadex LH-20 column. The dark green fraction that was eluted first was collected, then mixed with excess $NaSbF_6$ for 15 min. Insoluble products were collected after centrifugation. The final single crystals ($[Ag_x\ Au_{25-x}(PPh_3)_{10}(PET)_5Cl_2]^{2+}$ ($x \leq 13$)) were obtained from a mixed solution of DCM/diethyl ether.

Self-Assembly of Ag_xAu_{25-x}@FHO-Fe^{3+}

0.55mg of Ag_xAu_{25-x} was dissolved in 0.5mL of DCM and then added dropwise in the 5mL of FHO-Fe^{3+} aqueous solution (1 mg/mL) for stirring overnight. The final Ag_xAu_{25-}

$_x$@FHO/Fe^{3+} uniform dispension was obtained, suggesting the initial 0.55mg Ag_xAu_{25-x} has been almost completely solubilized into the FHO-Fe^{3+} micelles. Therefore, the loading rate of NCs can be approximately calculated as 10% (See the formula 1).

Loading rate (%)=Initial weight of NCs/(Weight of micelles+Initial weight of NCs) (1)

Catalytic Activity of FHO-Fe^{3+} Towards H_2O_2 for Producing O_2

The catalytic ability of FHO-Fe^{3+} on H_2O_2 for the generation of O_2 was monitored employing a portable dissolved O_2 instrument. The O_2 content in the mixed solution of H_2O_2 (0.03%)/FHO-Fe^{3+} (1mg/mL) was measured at a certain time interval (1 min). The two control groups with H_2O_2 (0.03%) or H_2O_2 (0.03%)/FHO (1mg/mL) were also separately implemented under the identical conditions. To simulate the real tumor environment, the pH value of the above test solutions were all adjusted to 5.5.

Laser-Induced Photothermal Conversion Effect

2mL of the various samples (FHO-Fe^{3+} in PBS, Ag_xAu_{25-x} in DMF, Ag_xAu_{25-x}@FHO/Fe^{3+} in PBS) at the same Ag_xAu_{25-x} (0.2mg) or FHO/Fe^{3+} (2mg) content were added in a 5mL glass bottle followed by irradiated with an 808 nm laser (1 W/cm^2) and recorded by the Fluke Ti32 thermal infrared camera immediately at regular time intervals (1min), respectively. The equal volume of PBS and DMF were used as controls.

Laser-Induced Photodynamic Effect

The photodynamic effects were tested by monitoring the absorption change of DPBF at 410 nm over specimens. Concretely, 1mL of DPBF (0.196 mg/mL) was mixed with 1 mL of PBS containing nothing, FHO-Fe^{3+}, Ag_xAu_{25-x}@FHO/Fe^{3+}, or Ag_xAu_{25-x}@FHO/Fe^{3+}+0.03% H_2O_2 at the same FHO-Fe^{3+} concentration (1mg/mL), or mixed with 1mL of DMF containing Ag_xAu_{25-x} (0.1mg/mL, same as the Ag_xAu_{25-x} content in Ag_xAu_{25-x}@FHO/Fe^{3+}) and then the absorption intensities at 410 nm of above mixture were measured at different periods of 808nm irradiation (1 W/cm^2) using a UV-3900 spectrophotometer, respectively.

Measurements of Cellular Singlet Oxygen ($^1O_2$) Generation

The intracellular $^1O_2$ productions of FHO-Fe^{3+}, Ag_xAu_{25-x}@FHO and Ag_xAu_{25-}

$_x$@FHO/Fe^{3+} in MCF-7 cells were examined by using the 2', 7'-dichlorofluorescein diacetate (DCFH-DA) as a $^1O_2$ fluorescence probe.[4] In briefly, MCF-7 cells were firstly seeded into a 24-well plate (10^4 cells/well) for 24 h incubation. Then the cell media were replaced with fresh one containing PBS, FHO-Fe^{3+}, Ag_xAu_{25-x}@FHO or Ag_xAu_{25-x}@FHO/Fe^{3+} (0.1mg/mL) for additional 6 h incubation, respectively. The cell media were instead fresh serum-free media containing DCFH-DA (10 μM) for 20 min incubation and selectively irradiated with a 1W/cm^2 808 nm laser for 10 min followed by immediately captured via an inverted fluorescence microscope (DMI3000B, Leica, German).

In Vitro Fluorescence Imaging (FI)

MCF-7 cells (10^5 cells/dish) were seeded onto glass-bottom cell culture dishes (Φ=35 mm, NEST) at 37°C for 12 h incubation. The cell culture medium was then instead 3mL of fresh medium containing Ag_xAu_{25-x}@FHO/Fe^{3+} (100 μg/mL) for further incubating for 3 h, respectively. The other two groups were pretreated by 100 μg/mL FA or both FA and HA (100 μg/mL) followed by the addition of Ag_xAu_{25-x}@FHO/Fe^{3+} (100μg/mL). Finally, the cells were washed with PBS for 3 times, then pictured under an Olympus FluoView FV1000 confocal microscope (60×oil objective) at the excitation wavelength of 568 nm.

Quantitative determination of the targeting effect of Ag_xAu_{25-x}@FHO/Fe^{3+} micelles

To study the targeting effect of Ag_xAu_{25-x}@FHO/Fe^{3+} on cancer cells, we selected MCF-7 cancer cells with over-expression of FA and CD44 receptors as the cell model, and selected HA and FA as inhibitors of FA and CD44 receptors. MCF-7 cells were seeded into a 24-well culture plate at a density of 10^5 cells/well and incubate for 24 h, which were divided into four groups. The culture medium of first three groups were then replaced with 0.5 mL of fresh medium containing HA (100 μg/mL), FA (100 μg/mL), or both HA/FA (100 μg/mL) for pretreatment. After 1h, the fresh medium containing Ag_xAu_{25-x}@FHO/Fe^{3+} micelles with the same concentration were added for further 2h incubation. The last group was directly treated by the fresh medium containing Ag_xAu_{25-x}@FHO/Fe^{3+} micelles for 2h. After the incubation, the stale medium were quickly discarded, cold PBS was added to realize the termination of

cell uptake and washed for 3 times. Finally, 200 μL of DI water was added to each well. The cells were scraped off and broken by ultrasound. The amounts of Au in each sample were measured using inductively coupled plasma mass spectrometry (ICP-MS) test. The Coomassie Brilliant Blue method is used to determine the protein content to eliminate errors caused by the different number of cells per well.[5] ??

In Vitro Photothermal Therapy (PTT)/Photodynamic Therapy (PDT) Cooperative Therapy

The phototherapy effects of different samples were compared. MCF-7 cells were seeded in 96-well plates (5×10^3 cells/well) for 24 h. Fresh culture media containing FHO-Fe^{3+}, Ag_xAu_{25-x}@FHO or Ag_xAu_{25-x}@FHO/Fe^{3+} at varied Ag_xAu_{25-x} and FHO-Fe^{3+} concentrations (0, 0.1, 0.2, 0.4 and 0.8 mg/mL of FHO-Fe^{3+}; 0, 0.01, 0.02, 0.04 and 0.08 mg/mL of Ag_xAu_{25-x}) were replaced to the stale culture media of the cells, respectively. After incubation for 4 h at 37℃, the cells were then treated with or without 808 nm laser irradiation (1 W/cm^2) for 10 min. Afterthat, the cells were incubated for further 24 h for the 3-(4, 5-dimethyl-2-thiazolyl)-2,5-diphenyl-2H-tetrazolium bromide (MTT) assay and Hoechst 33342/propidium iodide (PI) live/dead cell double staining assay.[6]

Determination of cell uptake of different micelles

Since the above MTT experiment used two different micelles, including Ag_xAu_{25-x}@FHO and Ag_xAu_{25-x}@FHO/Fe^{3+}, we need to investigate whether there is a big difference in the amount of cells taken up by different micelles to correct the above MTT results. MCF-7 cells were seeded into a 24-well culture plate at a density of 10^5 cells/well and incubate for 24 h. After the cells attachment, fresh medium containing the different concentration (100, 200, 400, 800 μg/mL) of Ag_xAu_{25-x}@FHO and Ag_xAu_{25-x}@FHO/Fe^{3+} were replaced the stale medium and incubated for 3h, respectively. After the incubation, the old medium was quickly discarded, ice cold PBS was added to stop the cell uptake, and the cell monolayer was washed by 3 times. Finally, 200 μL of DI water was added to each well. The cells were scraped off and broken by ultrasound. The amounts of Au in each sample were measured using ICP-MS test. The Coomassie Brilliant Blue method is used to determine the protein

content to eliminate errors caused by the different number of cells per well.[5] ⍰⍰

Animal Models

Kunming white mice were obtained from the Laboratory Animal Center of Anhui Medical University (Certification of quality 34000200000077, 34000200000078). 5×10^6 H22 cells were suspended in 100 μL of serum-free medium and injected into the back of hind leg of each mouse. This study was conducted in strict accordance with the recommendations in the Regulations on the Management of Laboratory Animals in China promulgated in 1988.

In Vivo FI

Model tumor mice were injected intravenously with Ag_xAu_{25-x}@FHO-Fe^{3+} at a dose of 6 mg/kg body weight, respectively. FI images were taken using a small animal in vivo optical imaging system (IVIS LuminaLT) after post-injection on tumor mice at 2h, 4h and 6h, respectively.

In Vivo biodistribution

H22 tumor-bearing mice were randomly divided into two groups followed by an intraperitoneal injection of Ag_xAu_{25-x}@HO and Ag_xAu_{25-x}@FHO-Fe^{3+} (10 mg/kg mice). The mice were euthanized at 6h, and the tumors and major organs were harvested. Then, the tumors and major organs were dispersed and digested in 5 mL of concentrated HNO_3 overnight followed by boiling at 100 °C. Finally, the remaining solution was cooled and diluted to 5 mL with DI water. After centrifugation and filtration, the clear solution is extracted. The amounts of Au in each sample were measured using ICP-MS test.

In Vivo PTT/PDT Cooperative Therapy

The model tumor mice were systemically administered with PBS, FHO/Fe^{3+}, Ag_xAu_{25-x}@FHO, and Ag_xAu_{25-x}@FHO/Fe^{3+} (6 mg/kg mouse weight) via tail vein injection. After 24 h post-injection, the tumor regions of living mice were exposed (10min) or unexposed to 808 nm laser (1 W/cm^2). Afterwards, the mice were weighted and the solid tumor sizes were measured by a caliper every 3 days. After one cycle experiment, the mice were carefully sacrificed, and the tumor tissues were collected and fixed for subsequent histological investigation, using a hematoxylin and eosin

(H&E) staining method. The pictures were obtained by an inverted fluorescence microscope.

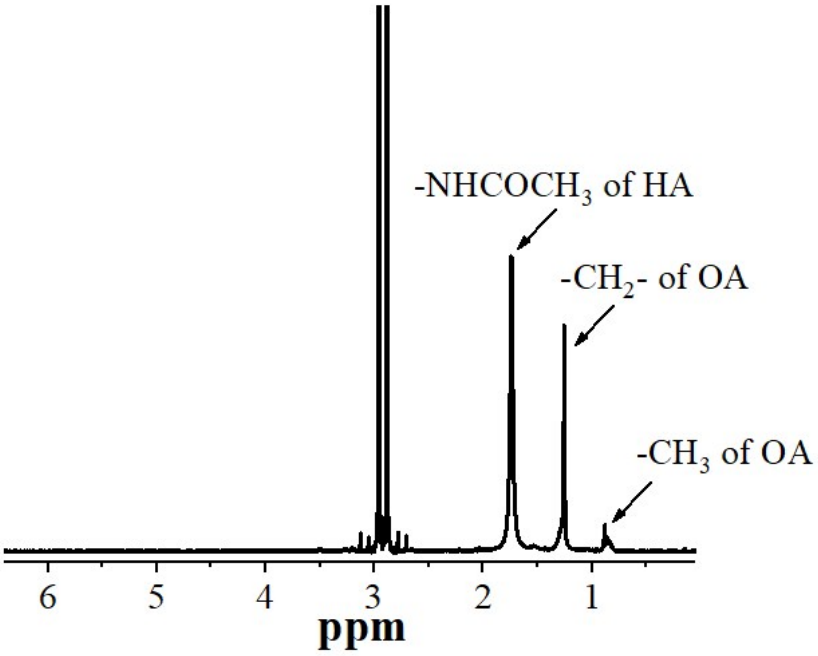

Fig. S1 ^{1}H NMR spectrum of HA-OA conjugate (HO). The peaks for the N-acetyl group (-$NHCOCH_3$) of HA and the partial methylene (-CH_2-) and methyl (-CH_3) groups of OA were confirmed. [7,8] The GR (%) of OA on HA was calculated by integrating the peak intensity of the −$NHCOCH_3$ group of HA and the peak intensity of the -CH_3 of OA, which was determined as 10.3%.

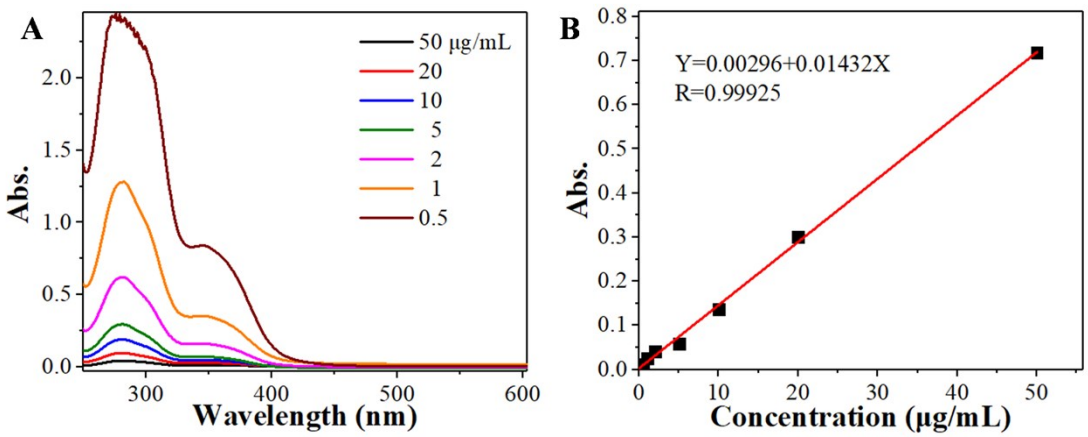

Fig. S2 (A) UV-Vis spectra and (B) Linear standard curve of FA with different FA concentrations at a wavelength of 360nm. The GR of FA in FHO measured by UV-Vis method was 11.8%.[2]

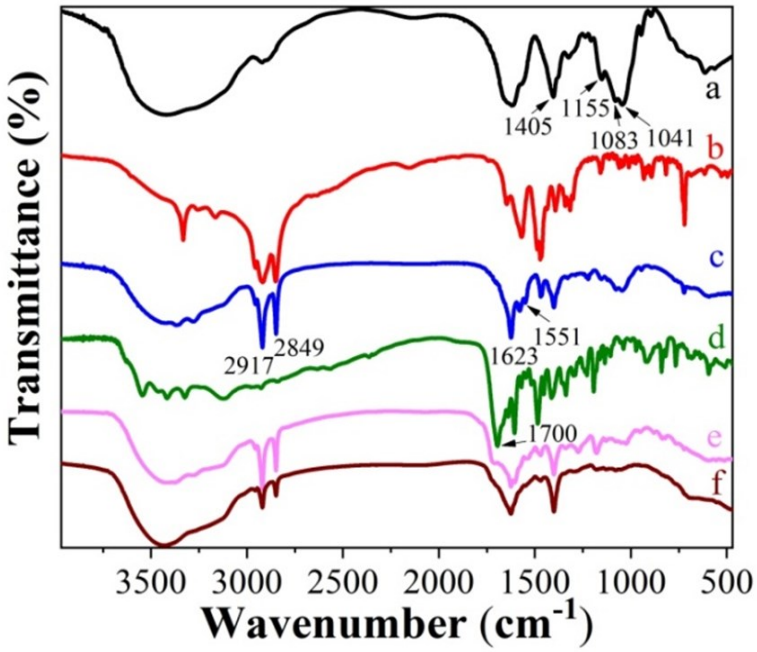

Fig. S3 FTIR spectra of (a) HA, (b) OA, (c) HO, (d) FA, (e) FHO and (f) FHO-Fe^{3+}. Comparing the FTIR spectrum of HO with that of HA, the original characteristic peaks of HA at 1405 cm^{-1} (-C=O), 1155 cm^{-1} (C-O-H), 1083 cm^{-1} (C-O), and 1041 cm-1 (C-O-C) still exist in the spectrum of HO,[9] furthermore, several new absorption bands, such as C–H stretching at 2917 and 2849 cm^{-1}, amide I and II bonds at 1623 and 1551 cm^{-1} also could be seen,[10-12] manifesting the successful bonding of HA and OA. After the

further conjugation of FA, a typical carboxyl group band of FA at 1700 cm^{-1} was observed from the FTIR spectrum of FHO, however, this absorption peak almost disappeared after the addition of Fe^{3+}, indicating the coordination of carboxyl groups with Fe^{3+} ions.

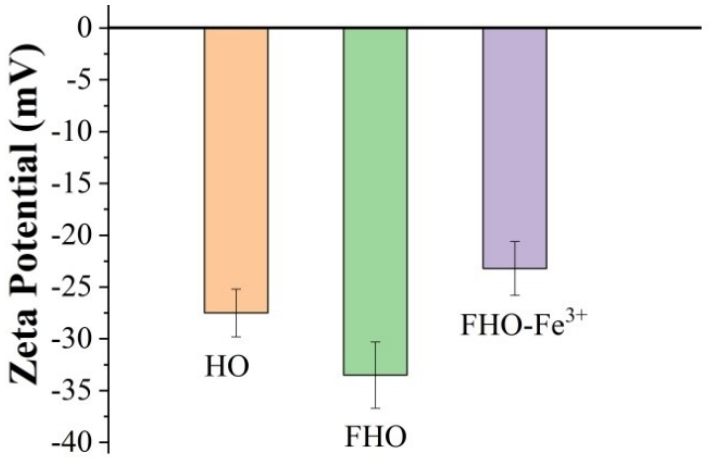

Fig. S4 Zeta potentials of HO, FHO and FHO-Fe^{3+}. The zeta potential is a typical indicator for dispersions.[13] Zeta potential values more negative or positive than 30 mV are generally deemed to represent sufficient mutual repulsion to ensure the stability of the solution. The results of maintaining at a desirable negative potential level demonstrated the stability of FHO-Fe^{3+} micelles.

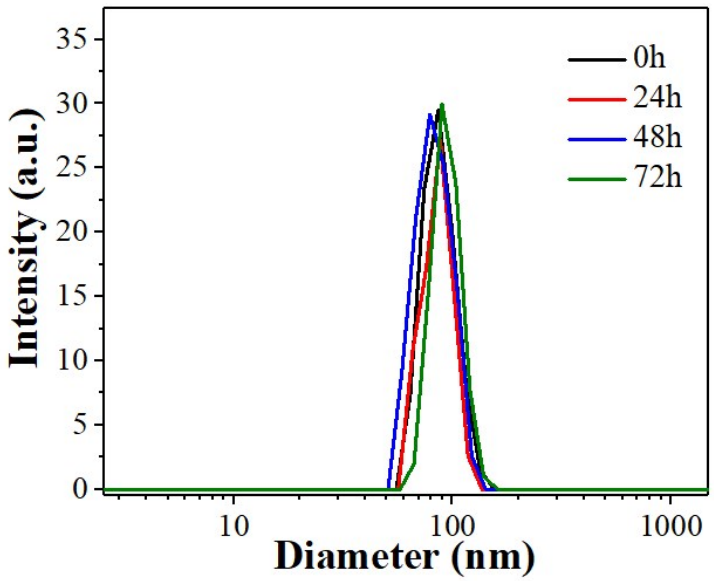

Fig. S5 Stability of FHO-Fe^{3+} micelles at 10% fetal bovine serum (FBS) via dynamic light scattering test. During body circulation, the serum stability of micelles in physiological environment is particularly important, so the particle size stability of

micelles at 37°C in 10% FBS medium was determined. After incubation in 10% FBS solution for 72 h, the particle size of FHO-Fe^{3+} micelles remained almost unchanged, indicating that the hydrophilic shell on the surface of FHO-Fe^{3+} micelles can help them avoid the adsorption of plasma proteins.[14]

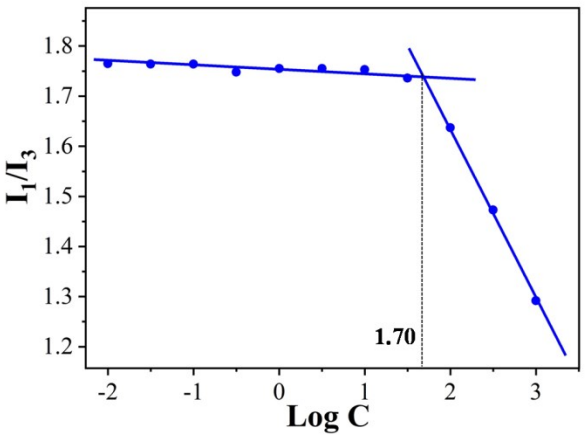

Fig. S6 Variation of fluorescence intensity ratio for I_1, 373nm/I_3, 384nm against logarithm of FHO-Fe^{3+} concentration. The CMC of the FHO-Fe^{3+} assemblies determined by fluorescence measurement using pyrene as a probe was calculated as 50.1 μg/mL in DI water.

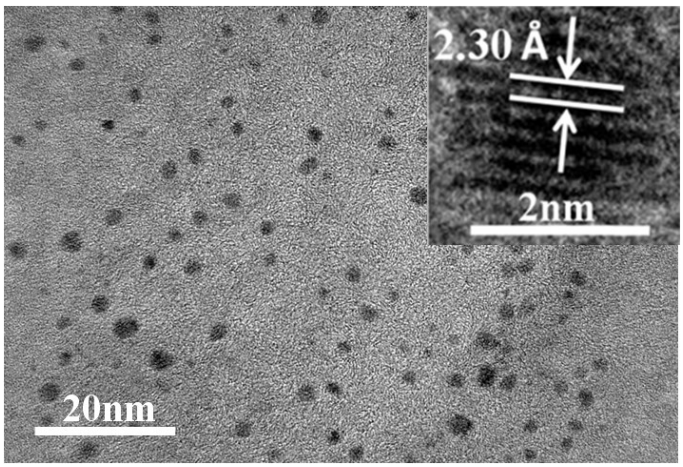

Fig. S7 TEM images of Ag_xAu_{25-x}; high-resolution TEM (HR-TEM) image of a single Ag_xAu_{25-x} (inset). The TEM image of bimetallic NCs Ag_xAu_{25-x} showed an average particle size of 2 nm; the HR-TEM image in the inset presents a single Ag_xAu_{25-x} with a discerned lattice spacing of 2.30 Å, which is in accord with metallic AuAg.[15]

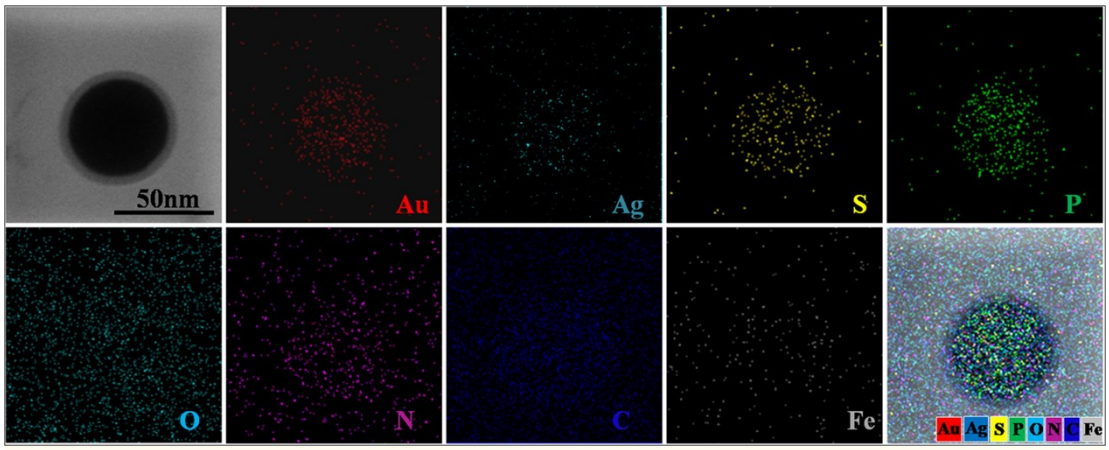

Fig. S8 Scanning TEM image of Ag_xAu_{25-x}@FHO-Fe^{3+} and the corresponding elemental mappings of Au, Ag, S, P, O, N, C and Fe.

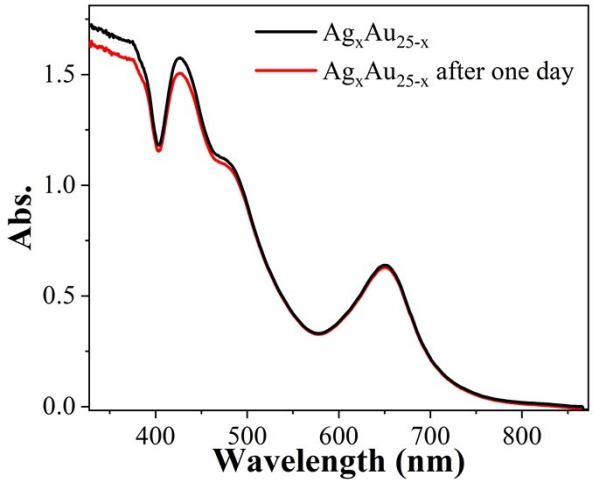

Fig. S9 UV-Vis spectra of Ag_xAu_{25-x} in DCM. After leaving for one day, no obvious changes were found in the UV-Vis spectra, showing the clusters have good stability and do not easy to agglomerate into large particles.

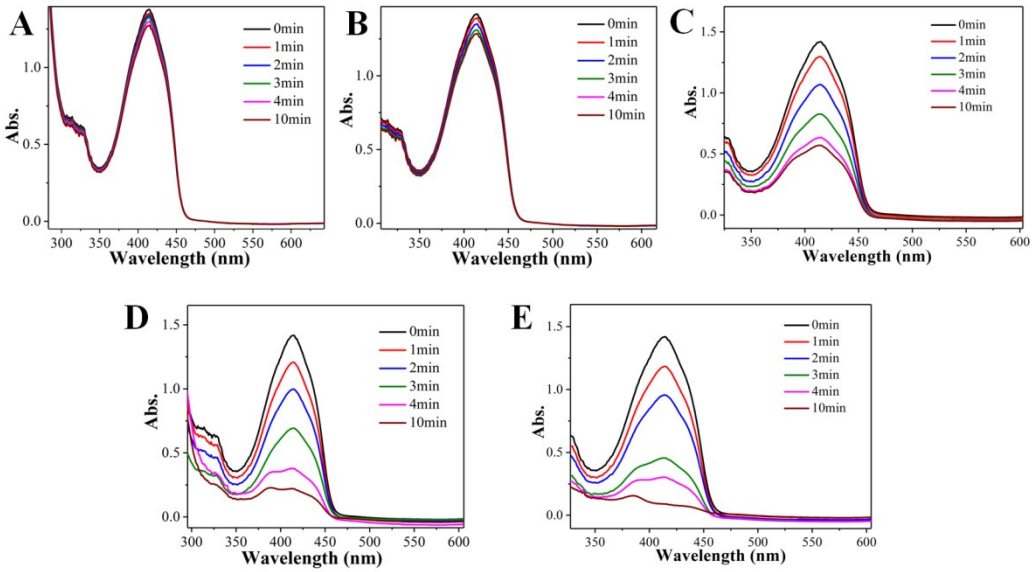

Fig. S10 The UV-Vis absorption spectra of (A) DPBF, (B) DPBF+FHO-Fe^{3+}, (C) DPBF+Ag_xAu_{25-x}, (D) DPBF+Ag_xAu_{25-x}@FHO-Fe^{3+} and (E) DPBF+Ag_xAu_{25-x}@FHO-Fe^{3+} +0.03%H_2O_2 recorded with irradiation (808nm, 1.0 W/cm^2) at different time. Little changes in absorbance of DPBF and DPBF/FHO-Fe^{3+} demonstrated they have been not affected by laser.

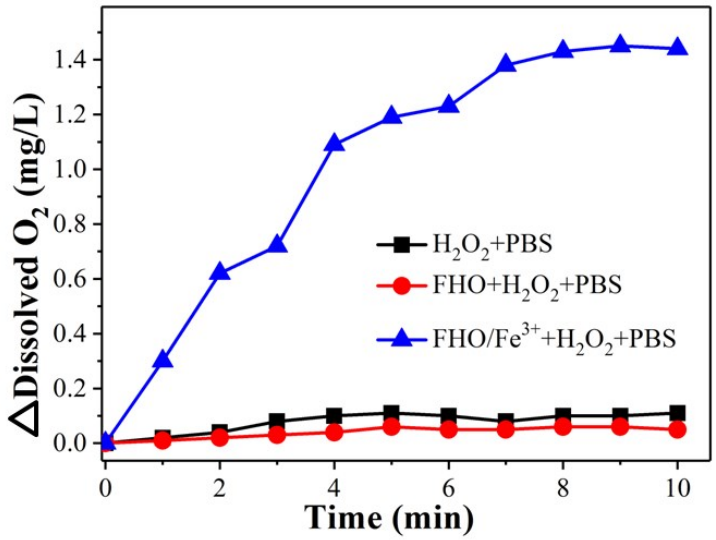

Fig. S11 The concentration changes of the dissolved O_2 in PBS (pH 5.5) with the addition of H_2O_2 (0.03%), FHO+H_2O_2 (0.03%) and FHO-Fe^{3+}+H_2O_2 (0.03%), respectively. O_2 is one of the main influencing factors of photodynamic effect. The production of large amounts of O_2 by the catalysis of FHO-Fe^{3+} towards H_2O_2 was significantly observed while almost no O_2 was generated in the H_2O_2 alone solution

and FHO/H_2O_2 solution, displaying the desirable catalytic activity of Fe^{3+} from FHO-Fe^{3+} on H_2O_2 for producing O_2.

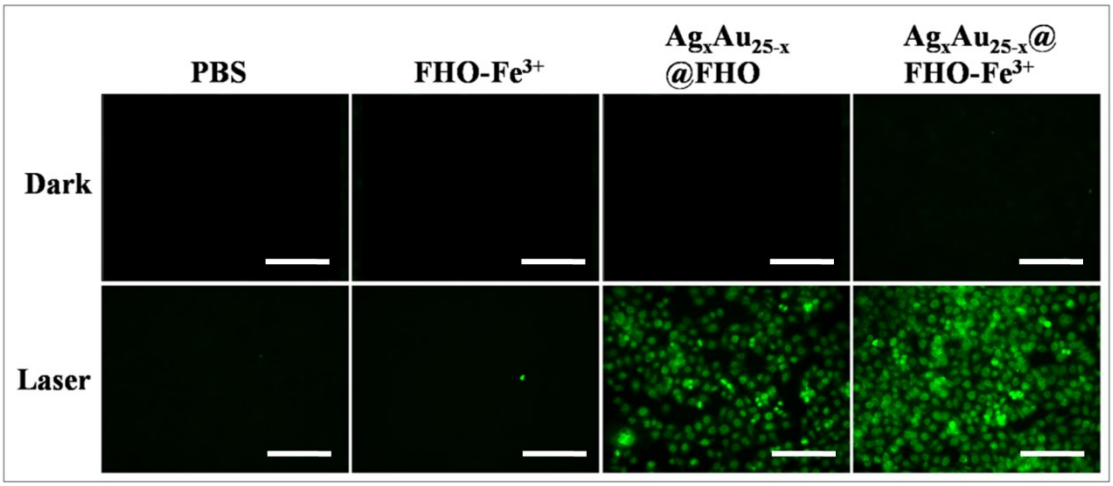

Fig. S12 Fluorescence microscopy images of MCF-7 cells that received different treatments (with various samples, with or without laser) as indicated. Green color represents $^1O_2$ indicator DCFH-DA (scale bar=200 μm). The 808 nm laser power intensity is 1 W/cm^2.

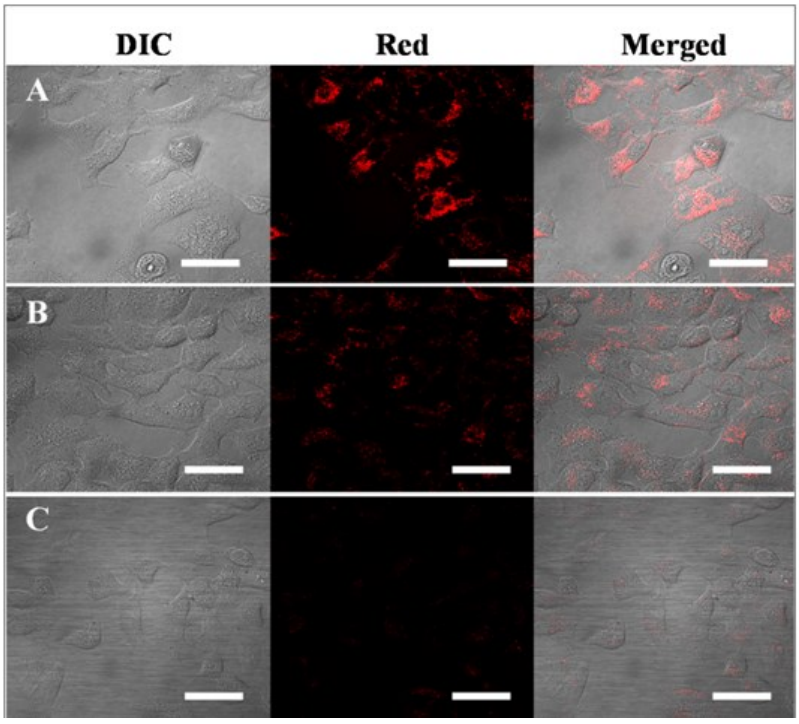

Fig. S13 CLSM images of MCF-7 cells pretreated by (A) nothing, (B) FA, (C) FA/HA after incubation with Ag_xAu_{25-x}@FHO-Fe^{3+} for 3 h, respectively. Images were captured in the differential interference contrast (DIC) mode and red channel. Scale bar: 20 μm. Firstly, MCF-7 cells that could express different levels of CD44 and FA

receptors were chosen for cell imaging. As expected, significant fluorescence signal was observed after a 3 h incubation of MCF-7 cancer cells with the Ag_xAu_{25-x}@FHO-Fe^{3+} (Fig. S13A), indicating the successful uptake of Ag_xAu_{25-x}@FHO-Fe^{3+} by MCF-7 cells. After MCF-7 cells were pretreated with free FA or FA/HA, for blocking FA receptor and CD44 on the cell surface (Figs. S13B-C), an obvious decrease in fluorescence intensity of Ag_xAu_{25-x}@FHO-Fe^{3+} in the MCF-7 cells could be seen due to the suppressed intracellular uptake effect. These results indicate the Ag_xAu_{25-x}@FHO-Fe^{3+} assemblies possessed capability of the receptor-mediated active targeted FI.

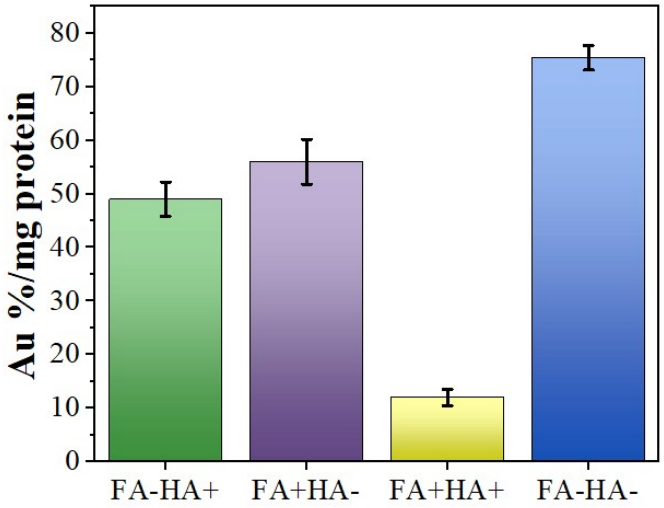

Fig. S14 Celluar uptake of Au in MCF-7 cells after incubated with Ag_xAu_{25-x}@FHO-Fe^{3+} (100μg/mL) for 2h with or without HA or FA pretreated. FA-HA+ represent only pretreated by HA; FA+HA- represent only pretreated by FA; FA+HA+ represented both pretreated by HA and FA; FA-HA- represented without any treatment. After pretreated by HA, FA or HA/FA, the amount of cell uptake of Ag_xAu_{25-x}@FHO-Fe^{3+} were greatly decreased compared to that of FA-HA- group, demonstrating the HA and FA corecepters-mediated endocytosis process of Ag_xAu_{25-x}@FHO-Fe^{3+}.

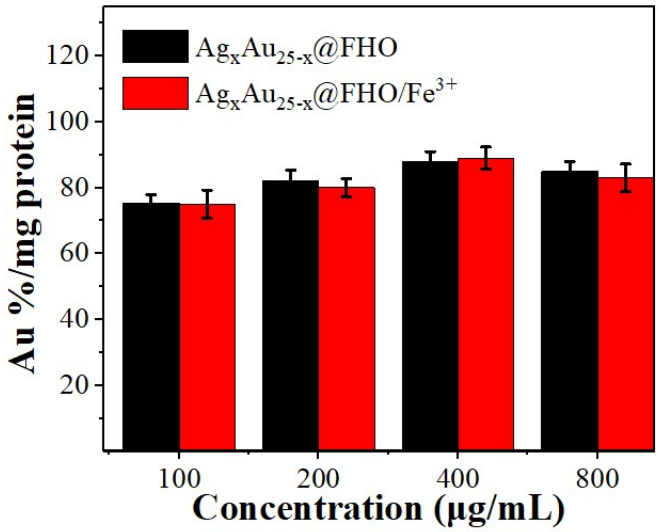

Fig. S15 Celluar uptake of Au in MCF-7 cells after incubated with Ag_xAu_{25-x}@FHO and Ag_xAu_{25-x}@FHO/Fe^{3+} for 3h with different concentrations (100, 200, 400, 800 μg/mL). It can be seen that there is no significant difference between the uptake efficiency of the Ag_xAu_{25-x}@FHO and Ag_xAu_{25-x}@FHO/Fe^{3+} micelles at different concentrations, indicating that the presence of a trace of Fe^{3+} did not affect the results of cell uptake. The main driving force of cell uptake is the receptor-mediated active targeting effect of micelles on cancer cells (Fig. S14).

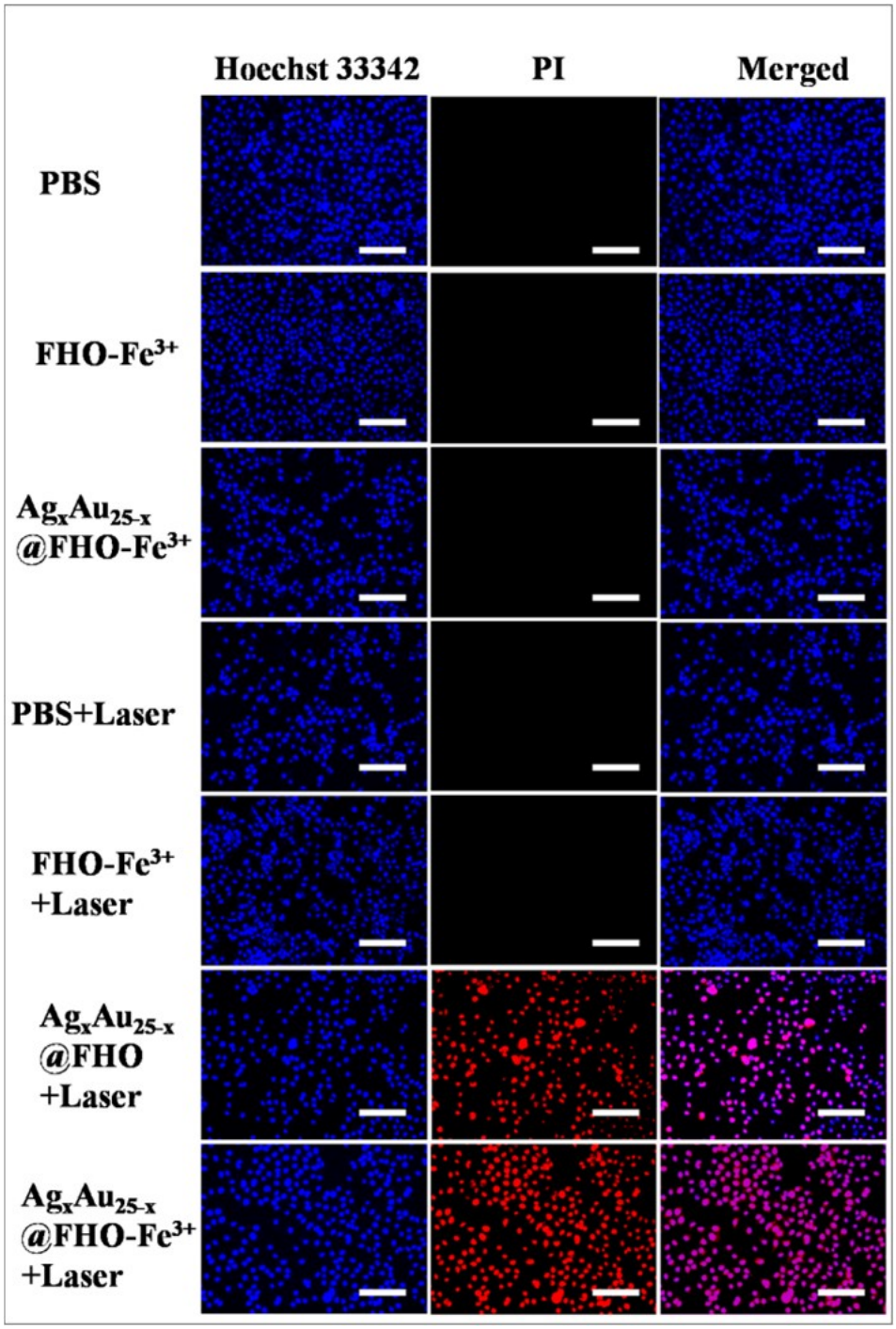

Fig. S16 Fluorescence microscopy images of MCF-7 cells incubated with different samples, without and with laser irradiation (808nm, 1.0 W/cm^2). The MCF-7 cells were dyed blue with Hoechst 33342 (left) and red by PI (middle), and the merged images are also shown (right). The scale bars are 200 μm. Here, blue, black and merged images can be observed from the groups of PBS, FHO-Fe^{3+} and Ag_xAu_{25-x}@FHO-Fe^{3+}, indicating their favorable biocompatibility. However, upon the 808nm laser irradiation, apparent cell deaths were observed when co-incubated with

Ag_xAu_{25-x}@FHO and Ag_xAu_{25-x}@FHO-Fe^{3+} owing to the synergistic PTT/PDT effects while red fluorescence signal still rarely can be seen from that group of FHO-Fe^{3+}. In addition, the group of Ag_xAu_{25-x}@FHO-Fe^{3+} emerged much brighter red fluorescence owing to the excess production of O_2-enhanced PDT by Fe^{3+} of Ag_xAu_{25-x}@FHO-Fe^{3+}.

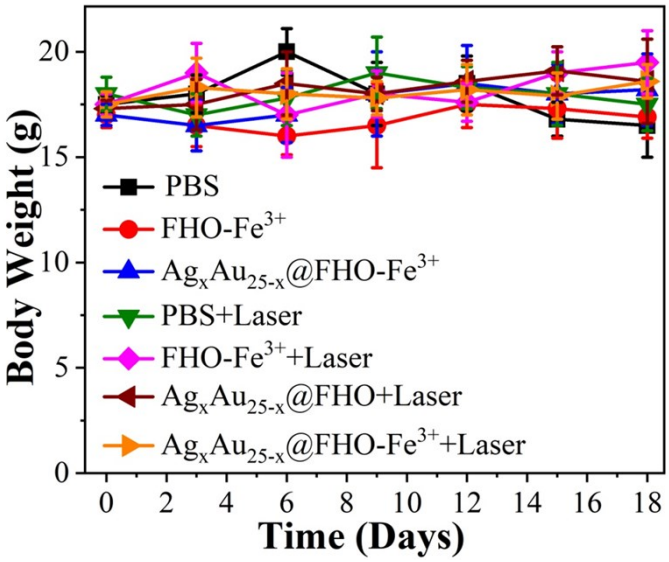

Fig. S17 Body weight of the mice after different treatments.

Reference

1 M. Wilhelm, C. L. Zhao, Y. Wang, R. Xu, M. A. Winnik, J. L. Mura, G. Riess and M. D. Croucher, *Macromolecules,* 1991, **24**, 1033-1040.

2 Y. Zheng, Z. Cai, X. Song, Q. Chen, Y. Bi, Y. Li and S. Hou, *J. Drug Targeting.*, 2009, **17**, 294-303.

3 S. Wang, X. Meng, A. Das, T. Li, Y. Song, T. Cao, X. Zhu, M. Zhu and R. Jin, *Angew. Chem. Int. Edit.,* 2014, **53**, 2376-2380.

4 N. A. Daghastanli, R. Itri and M. S. Baptista, *Photochem. Photobiol.*, 2008, **84**, 1238-1243.

5 M. P. Goren and J. T. Li, *Clin. Chem.*, 1986, **32**, 386-388.

6 Y. Yang, Y. Wang, W. Xu, X. Zhang, Y. Shang, A. Xie and Y. Shen, *Eur. J. Inorg. Chem.*, 2017, **15**, 2236-2246.

7 L. Qiu, M. Zhu, Y. Huang, K. Gong and J. Chen, *RSC Adv.*, 2016, **6**, 39896-39902.

8 S. Uthamana, A. P. Mathew, H. J. Park, B. Lee, H. S. Kim, K. M. Huh and I. K. Park, *Carbohyd. Polym.*, 2018, **181**, 1-9.

9 Y. Yang, S. Wang, C. Wang, C. Tian, Y. Shen and M. Zhu, *Chem. Asian J.,* 2019, **14**, 1418-1423.

10 J. Li, Y. Shu, T. Hao, Y. Wang, Y. Qian, C. Duan, H. Sun, Q. Lin and C. Wang, *Biomaterials*, 2013, **34**, 9071-9081.

11 M. Motiei and S. Kashanian, *Eur. J Pharm. Sci.*, 2017, **99**, 285-291.

12 Y. Luan, M. Yang, Q. Ma, Y. Qi, H. Gao, Z. Wu and G. Wang, *J Mater. Chem. A*, 2016, **4**, 7641-7649.

13 K. Jasuja and V. Berry, *ACS Nano*, 2009, **3**, 2358-2366.

14 C. L. Lo, C. K. Huang, K. M. Lin and G. H. Hsiue, *Biomaterials*, 2007, **28**, 1225-1235.

15 Y. Xu, L. Liu, H. Chong, S. Yang, J. Xiang, X. Meng and M. Zhu, *J Phys. Chem. C,* 2016, **120**, 12446-12451.